Title	Effects of specimen size and boundary conditions on the penetration depth of metal ceramic structure
Author(s)	Liu, Jianfei; Yuan, Jianming
Citation	Liu, J., & Yuan, J. (2014). Effects of specimen size and boundary conditions on the penetration depth of metal ceramic structure. Procedia engineering, 75, 71-77.
Date	2013
URL	http://hdl.handle.net/10220/20959
Rights	© 2013 The Authors. Published by Elsevier Ltd. This is an open access article under the CC BY-NC-ND license (http://creativecommons.org/licenses/by-nc-nd/3.0/).

Available online at www.sciencedirect.com

ScienceDirect

Procedia Engineering 75 (2014) 71 – 77

Procedia Engineering

www.elsevier.com/locate/procedia

MRS Singapore - ICMAT Symposia Proceedings

7th International Conference on Materials for Advanced Technologies

Effects of Specimen Size and Boundary Conditions on the Penetration Depth of Metal Ceramic Structure

Jianfei Liu*, Jianming Yuan

Temasek Laboratories, Nanyang Technological University, 50 Nanyang Drive, Singapore 637553

Abstract

Ceramics has high hardness but low density and has been used in defense to enhance the protection of human bodies or vehicles against projectile penetration. Ceramics can defeat a ballistic threat by deforming and fracturing a metal projectile, thus eliminate or reduce the depth of penetration in backing steel. This study investigates the penetration progress of a tungsten alloy projectile into an Al_2O_3 ceramics (alumina) backed with high strength steel 4340. Depth of penetration tests were conducted on ceramics/steel specimens by WNiFe projectiles at impact speeds around 1280m/s. Numerical simulations corresponding to the test configurations were carried out using commercial software (Autodyn) and the prediction of crater profile coincides with experimental results. Further simulations investigated the effects of specimen size and boundary conditions on the total depth of penetration; the performance of metal ceramic structure against ballistic penetration was explored and evaluated.

Keywords: Ballistic testing; Armor ceramics; Penetration depth; Numerical simulation.

1. Introduction

Ceramic materials or ceramic-based armors have been used to enhance the protection of aircraft, soldiers or vehicles. The most common ceramics being used in armors are inclusive of alumina (Al_2O_3) and Silicon carbide (SiC). Compared to steel, ceramics possesses characteristics of higher hardness but lighter density. The

* Corresponding author. Tel.: +65-65922607; fax: +65-65922607.
E-mail address: jianfeiliu@ntu.edu.sg

doi:10.1016/j.proeng.2013.11.014

high hardness of a ceramic improves its ability to resist ballistic penetration of high speed projectiles. If the hardness is sufficient high enough, a ceramics can cause the impacting projectile to be fractured and defeated before it penetrating through. Ballistic performance of ceramics has been studied extensively, and depth of penetration was usually used as a measure to evaluate the penetration performance [1, 2]. Previous studies include investigations on the effect of front plate and confinement, thickness of ceramics, composition and armor structural system, type of projectile, multi-layered ceramics and specimen scale on the failure mechanism and ballistic performance [3-10]. Computational simulations were also carried out [11, 12] and a novel element removal scheme for ceramics was introduced [13]. Extremely high speed penetrations on ceramics by large length-to-diameter ratio projectile were also undertaken via reverse ballistic tests [14-18]. This study focuses on the penetration progress of a tungsten alloy projectile into alumina ceramics and high strength steel 4340 at an impact speed around 1280m/s. Experiments using a two stage gas gun and numerical modeling via Autodyn were performed and their results on the crater profile were compared. Further numerical simulations verified the size effect and corresponding boundary conditions on the overall ballistic performance of the metal ceramics specimens.

2. Depth of penetration test and simulation

The depth of penetration test was carried out using a two stage gas gun. Configuration of the projectile and specimen (target) is illustrated in Fig.1. A cylindrical Al_2O_3 ceramics (R_c=51mm, L_c=25.5mm) was embedded and glued to a cylindrical 4340 backing steel (R_s=76mm, L_s=152mm). A flat nose cylindrical tungsten alloy rod (W4%Ni3%Fe, diameter 8.3mm, length 96.4mm) was propelled and impacted normally on the ceramic/steel specimen along its central line (x axis), at a speed of 1283m/s. Photos of the tested specimen showed that the ceramics was fully penetrated, resulting a residual penetration crater in the backing steel. The total penetration depth (TD) is defined as the difference between the length a and the specimen length L_s, and was measured as 57.43mm; and the average diameter ϕd of the crater is around 16.9mm. To show the role of ceramics in armor defense, a reference test with the same projectile at a speed of 1280m/s on a pure 4340 steel cylinder was conducted and the penetration depth was measured around 50.84mm. As density of the ceramics (99.5% Al_2O_3) is only 3.89g/cm^3, this largely reduces the areal density of the target without losing its capability in resisting ballistic penetration.

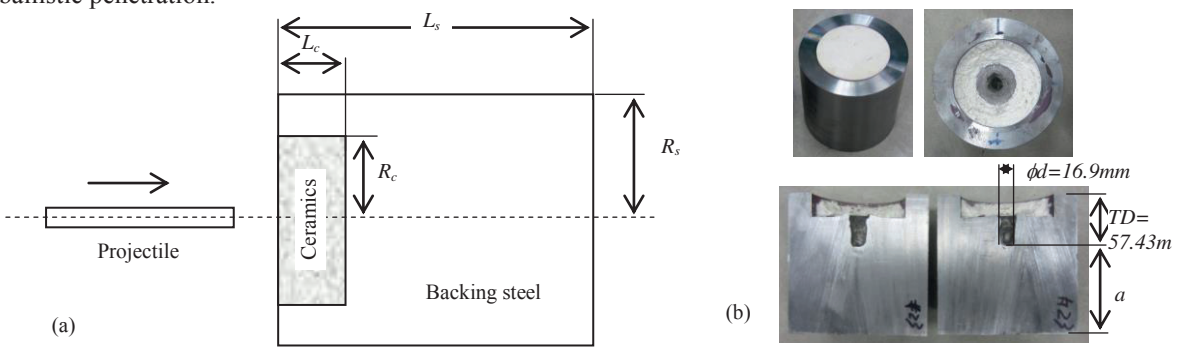

Fig. 1. (a) Schematic drawing of the ballistic test configuration and (b) photos of the tested specimen.

Corresponding to the configuration of testing, numerical simulation was performed to investigate the impact progress and responses of ceramic and backing steel. To save computational time, a 2D axial symmetrical model was constructed and solved using the commercial simulation software Ansys/Autodyn (Fig.2a). The projectile and ceramics were modeled by SPH (smoothed particle hydrodynamic) parts with particle size 0.5mm. The cylindrical backing steel was represented by a Lagrange part with geometry erosion of 2.0; mesh

size is 0.5mm around the impact region of R51x76mm and then gradually biased to 1mm at specimen outer surfaces. Constrained boundary (fixed in x direction) is applied on the right end surface of the cylindrical backing steel, to represent the boundary conditions of testing. The simulation was carried out from commencement of impact till 0.2ms, which encompasses the whole penetration progress till rest/rebound of the projectile. From the simulation results (Fig.2b), it was calculated that the final total penetration depth is TD=60.40mm and average crater diameter ϕd=16.4mm, which are quite close to the experimental results.

To investigate the penetration progress, three monitoring points (gauges, as indicated in Fig.2a) are placed respectively along the center line of the projectile and the outer side surface of the backing steel. In Fig.3a, the x velocities of gauge #5 and #6 on projectile dropped quickly when the particles of these monitoring points reached the impact interface. It is noted that the x velocity of gauge #4 almost kept its initial velocity and started to drop abruptly at around 0.1ms towards zero, which led to a full stop of the residual projectile. As there is a short portion of residual projectile after penetration in this simulation, this indicates the end of the penetration progress and the total duration is about 0.136ms. These profiles of x velocity demonstrate the distributions and variations of particle velocities along a projectile during a penetration, and show that for a long rod projectile, severe deceleration only occurs when the particles come into the impact interface.

Likewise, the other interesting phenomenon is the development and variations of temperature along the projectile during a penetration. As shown in Fig.3b, the project tip (gauge #6) and middle portion (gauge #5) become molten (melting temperature 2263K, as prescribed by the model) upon involved into the impact interface and continue to increase to even higher temperatures. However, temperature of the project butt (gauge #4) increases gradually and only reached 475K at the end of the simulation (0.2ms). This demonstrates that particle temperature is generated by the high adiabatic deformation of projectile front at impact interface; conduction of heat has less effect for such transient penetration progress.

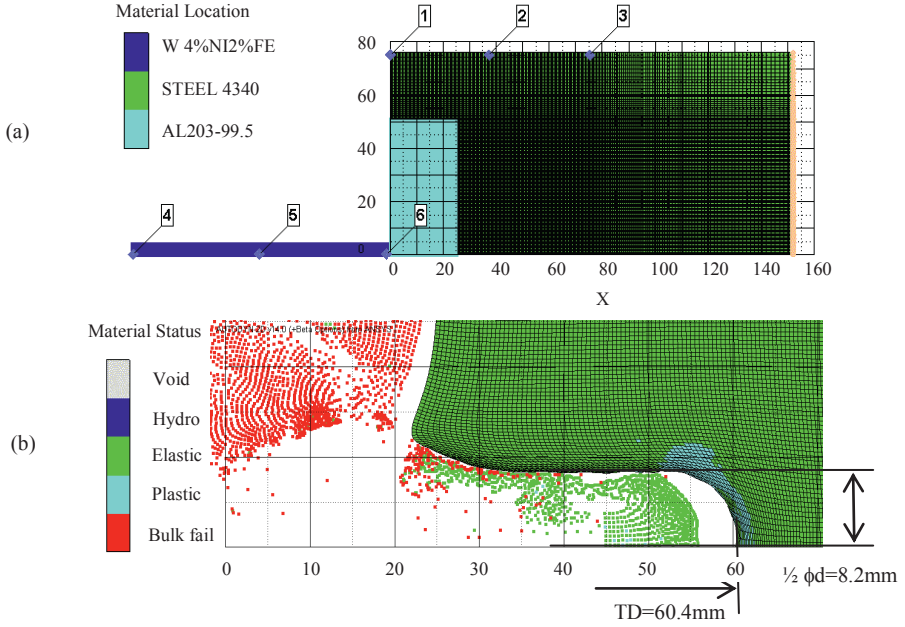

Fig. 2. 2D axial symmetric modeling of the depth of penetration testing using AUTODYN; (a) material locations before testing and (b) material status after penetration (at instant of 0.2ms).

During the penetration, lateral expansion of the ceramic and backing steel occurs due to the intrusion of the long rod into the target. In this simulation, velocity boundary condition was set on the end surface of the

backing steel with fixed value (V_x=0); this corresponds to the actual testing configurations. Therefore, amplitude of the lateral displacements of the backing steel cylinder is a measure to reflect whether the lateral size of the sample is sufficient to represent the target as a laterally infinite field. Fig.3c shows the lateral displacements of the three gauges (#1, #2, and #3) set on the outside of the backing steel. It is seen that the profiles fluctuate and reach maximum expansion value around 0.09mm. The profile of gauge #1 shows clearly the three major fluctuations with periodical duration around 0.04-0.05ms. As prescribed in the model of the sound speeds (10560m/s for ceramic and 5782m/s for backing steel), these lateral fluctuations should be corresponding to the transient transverse wave propagating to and reflected back from the backing steel's outside surface.

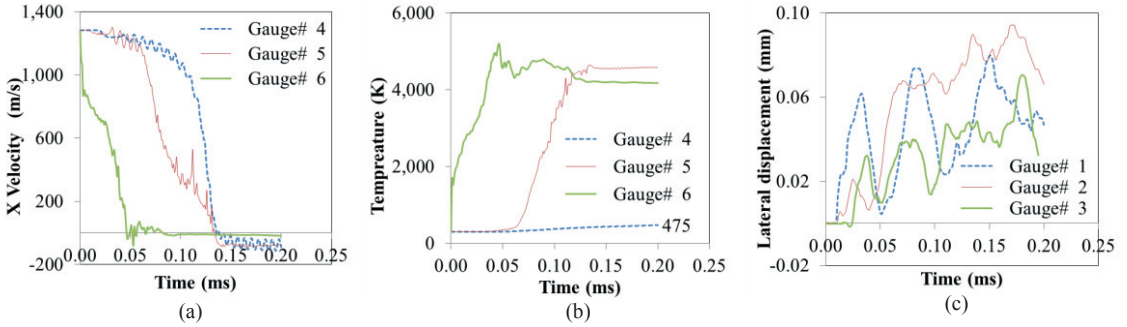

Fig. 3. (a) velocities and (b) temperatures of gauges on the projectile and (c) lateral displacement of gauges on the backing steel.

3. Effects of specimen size and boundary conditions on total penetration depth

During a ballistic penetration progress, the intrusion of projectile will induce severe deformations adjacent to the crater in the backing steel. Figure 4 shows the material status corresponding to the penetration testing, at the instant of 0.125ms when the plastic region in backing steel reaches the outmost. Outside this region (around ϕ45mm and length 100mm), material in the backing steel still responds elastically. In this case, it seems that this specimen size is sufficiently large that it may be regarded as a semi-infinite entity – the boundary conditions will be far-field constraints that will not affect total penetration depth as well as crater profile. To verify this, boundary condition in the simulation (the fixed backing boundary as shown in Fig. 4) was removed and the model of same size and meshes was recalculated with free boundary conditions (no constraints on its outside surfaces); the simulation outcomes actually reproduce the same results: total penetration depth 60.4mm and mean crater diameter 16.4mm.

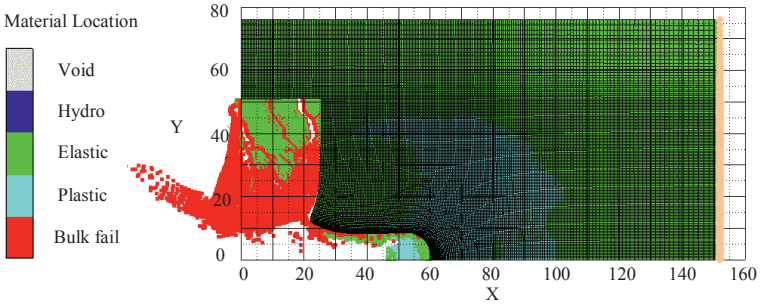

Fig. 4. The cracking in ceramics and upmost plastic region in backing steel (at instant of 0.125ms).

When the specimen is of limit size, the penetration depth will be affected and the boundary conditions to specimen will have effects on the penetration results. To quantify these effects, a series of simulations were

undertaken for models of different specimen sizes and boundary conditions; the projectile keeps same in material and profile as well as impact velocity (1280m/s). To verify the size effect, two configurations were considered for the models: one explores the effect of specimen lateral dimension, where specimen radius R_s varies from 21mm to 76mm while keeping its length L_s fixed at 152mm; the other explores the effect of specimen length, where specimen length L_s varies from 70mm to 152mm while keeping its radius R_s fixed at 76mm. To verify the effect of boundary conditions, three configurations were considered for the models: the first is free boundary condition where no constraint applied on specimen; the second is fixed backing boundary where x velocity is set to zero for the cylinder right end surface; and the third is fixed lateral boundary where the x and y velocities are set to zero for the cylindrical outer surface. For the free boundary condition, the total penetration depth should decrease with the increase of specimen size, and tends to converge to the value where semi-infinite condition reaches. Before specimen size is sufficient large, the total penetration will be greatly affected by the boundary conditions applied. Fig. 5 illustrates the penetration results for a short specimen (L_s=70mm) while its lateral size is sufficient large (R_s =76mm). It is seen that for a less thick specimen (e.g. backing panel), the penetration depth increases greatly (Fig. 5a, *TD*=71.20mm); the fixed backing boundary quite over strengthens the model (Fig. 5b, *TD*= 61.06mm); the fixed lateral boundary has less effect on the total penetration depth (Fig. 5c, *TD*=71.80mm), because the lateral size is sufficient large.

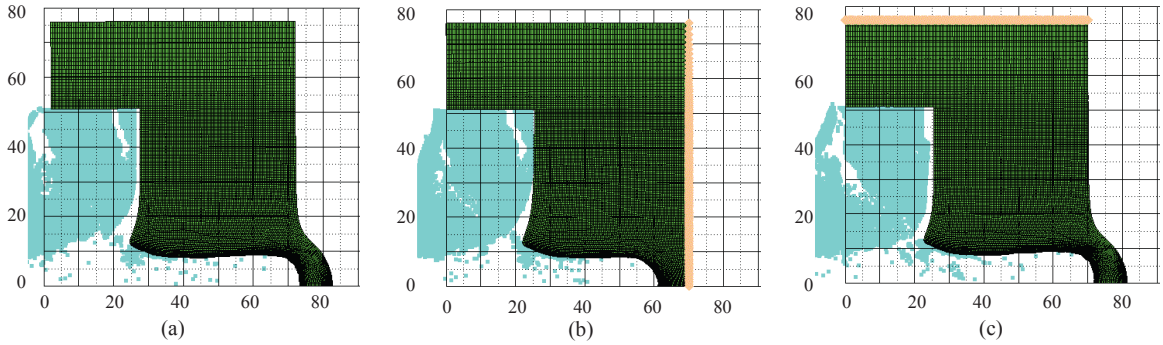

Fig. 5. Illustration of the effects of (a) free (b) fixed backing and (c) fixed lateral boundary conditions on the total penetration depth for a radius 76mm length 70mm cylindrical specimen (at instant of 0.2ms).

From the simulations, results of the total penetration depth (TD) for specimens with different radius R_s and different length L_s were obtained. For specimens with radius from 21mm to 51 mm, there is no steel flange confining the ceramic. The result shows specimens of small diameter or short length will result in large total penetration depth. If setting the total penetration depth (*TD*=60.40mm) of the specimen (radius 76mm and length 152mm – the tested specimen's size) as a reference value, the relative variation (*RV*) of different models can be calculated. Positive value of *RV* denotes that the *TD* is larger than the reference value. Fig. 6 shows the trend of this relative variation (*RV*) with the sizes of specimen and boundary conditions. The curves demonstrate clearly the tendency of convergence when specimen size increases, and the over or under estimation of *TD* if different boundaries are applied on small sized specimens. When the specimen size is beyond dimensions around diameter 50mm and length 100mm, the relative variation tends to be negligible; this actually coincides with the size of the upmost plastic region in backing steel during the penetration, as shown in Fig.4. The effects of size and boundary conditions demonstrate the importance that (1) a proper size of specimen should be selected according to the application requirements; and (2) accordingly, a proper jig or fixation mechanism should be used to conduct the experiments; lastly, (3) proper boundary conditions should be applied to the simulation model in order to correctly represent the applications as well as the experiments.

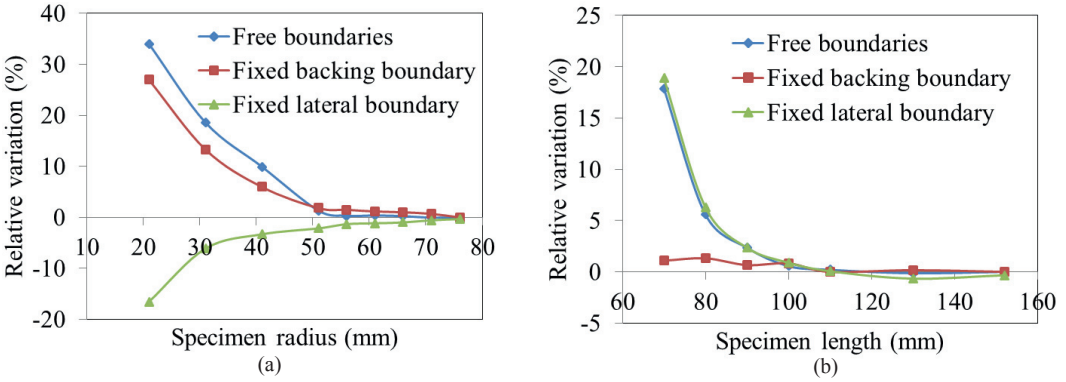

Fig. 6. The relative variation of total penetration depth of specimens with (a) different radius and (b) different length under different boundary conditions.

4. Conclusion

Ballistic penetration tests were conducted on ceramics block backed with 4340 steel. Cylindrical projectiles of tungsten alloy rod were used and launched by a two stage gas gun at a speed around 1280m/s. Numerical Autodyn models were established and corresponded to the experimental setup. The simulation results showed good agreement with the experimental results according to crater depth and diameter. Further investigations were carried out through numerical simulations, to understand the effects of specimen size and boundary conditions on the ballistic performances in terms of the total penetration depth. It is found that when specimen size is limited, subjected to the same threat level of a projectile, the penetration depth varies and the boundary conditions applied in simulation may result in over or under estimation in predictions. The minimum specimen size that results a specimen free from the effect of boundary constraints, is related to the maximum plastic region that is experienced by the specimen during a penetration.

5. Acknowledgement

This work was funded by Temasek Laboratories@NTU, Nanyang Technological University, Singapore under contract No. TL-9010101538-03. The authors also want to express acknowledgement to Professor Geoffrey E.B.Tan (from school of materials science and engineering, Nanyang Technological University) for his valuable inputs.

References

[1] Anderson, Jr. C.E., Royal-Timmons, S.A., 1997. Ballistic Performance of Confined 99.5%-Al2O3 Ceramics Tiles. Int J Impact Engng 19, p.703.
[2] Hohler, V., Stilp, A.J., Weber, K., 1995. Hypervelocity Penetration of Tungsten Sinter-alloy Rods into Aluminum. Int J Impact Engng 17, p.409.
[3] Tan, Z.H., Han, X., Zhang, W., Luo, S.H., 2010. An Investigation on Failure Mechanisms of Ceramic/metal Armour Subjected to the Impact of Tungsten Projectile. Int J Impact Engng 37, p.1162.
[4] Lee, M., Yoo, Y.H., 2001. Analysis of Ceramic/metal Armor Systems. Int J Impact Engng 25, p.819.
[5] Medvedovski, E., 2010. Ballistic Performance of Armour Ceramics: Influence of Design and Structure: Part 1. Ceramics International 36, p.2103.
[6] Medvedovski, E., 2010. Ballistic Performance of Armour Ceramics: Influence of Design and Structure: Part 2. Ceramics International 36, p.2117.

[7] Espinosa, H.D., Bras, N.S., Yuan, G., Xu, Y., Arrieta, V., 2000. Enhanced Ballistic Performance of Confined Multi-layered Ceramic Targets Against Long rod Penetrators through Interface Defeat. International Journal of Solids and Structures 37, p.4893.
[8] Shockey, D.A., Marchand, A.H., Skaggs, S.R., Cort, G.E., Burkent, M.W., Parker, R., 1990. Failure Phenomenology of Confined Ceramic Targets and Impacting Rods. Int J Impact Engng 9, p.263.
[9] Lundberg, P., Westerling, L., Lundberg, B., 1996. Influence of Scale on the Penetration of Tungsten Rods into Steel-backed Alumina Targets. Int J Impact Engng 18, p.403.
[10] Partom, Y., Littlefield, L., 1995. Validation and Calibration of a Lateral Confinement Model for Long-rod Penetration at Ordnance and High Velocities. Int J Impact Engng 17, p.615.
[11] Wilkins, M.L., 1978. Mechanics of Penetration and Perforation. Int J Engng Sci 16, p.793.
[12] Hayhurt, C.J., Clegg, R.A., Livingstone, I.H., Francis, N.J., Sep.1996. The Application of SPH Techniques in Autodyn-2D to Ballistic Impact Problems. 16th International Symposium on Ballistics, San Francisco, CA, p.23-28.
[13] Simha, C.H.M., Bless, S.J., Bedford, A., 2002. Computational Modeling of the Penetration Response of a High-purity Ceramic. Int J Impact Engng 27, p.65.
[14] Grace, F.I., Rupert, N.L., 1997. Analysis of Long Rods Impacting Ceramic Targets at High Velocity. Int J Impact Engng 20, p.281.
[15] Orphal, D.L., Franzen, R.R., Piekutowski, A.J., Forrestal, M.J., 1996. Penetration of Confined Aluminum Nitride Targets by Tungsten Long Rods at 1.5-4.5km/s. Int J Impact Engng 18, p.355.
[16] Orphal, D.L., Franzen, R.R., 1997. Penetration of Confined Silicon Carbide Targets by Tungsten Long Rods at Impact Velocities from 1.5 to 4.5km/s. Int J Impact Engng 19, p.1.
[17] Subramanian, R., Bless, S.J., 1995. Penetration of Semi-infinite AD995 Alumina Targets by Tungsten Long Rod Penetrations from 1.5 to 3.5 km/s. Int J Impact Engng 17, p.807.
[18] Westerling, L., Lundberg, P., Lundberg, B., 2001. Tungsten Long-rod Penetration into Confined Cylinders of Boron Carbide at and above Ordnance Velocities. Int J Impact Engng 25, p.703.